

## Improving energy-efficiency of pumping operations in waterways: a combined laboratory and computational approach

J. Hardy<sup>1</sup>, P. Dewallef<sup>1</sup>, S. Erpicum<sup>1</sup>, P. Archambeau<sup>1</sup>, M. Piroton<sup>1</sup>,  
D. Parkinson<sup>2</sup>, N. Taylor<sup>2</sup>, C. Barnett<sup>2</sup>, B. Dewals<sup>1</sup>  
<sup>1</sup> Université de Liège, Liège, Belgique  
joris.hardy@uliege.be

<sup>2</sup> Canal and River Trust, Milton Keynes, United-Kingdom

### Abstract

Pumping in waterways, particularly in artificial canals, is energy-intensive, costly and may be responsible for the emission of large quantities of CO<sub>2</sub>. Innovative pumping technologies have the potential to reduce energy consumption; but their performance needs to be thoroughly assessed. This communication presents the results of an experimental test bench for evaluating the performance of large submersible and dry-action centrifugal pumps typically used in waterways. It enables calibrating a pump numerical model. This computational model is challenging due to its non-linearity. The coupling of an induction motor with a pump operation model is innovative in the waterways field and especially, the identification of model parameters for large pump based on experimental data.

**Keywords:** Experimental pump test bench, Waterways pumps, Computational pump modelling, Pump calibration via optimization, Off-design pump operation characterization

## 1. INTRODUCTION

A suitable tool to evaluate the actual on-site energy efficiency of pumping systems used in waterways is missing. Indeed, pump manufacturers generally provide detailed information on a curve of pump efficiency at nominal rotation speed. In contrast, no or little information is available concerning off-design pump operation for varying speed, while variable speed drives are known to enable increasing the overall efficiency of the pumping system, which is precisely what matters for the end-users. A hybrid modelling approach is presented here. It involves a large experimental test bench (Hardy et al, 2021) used for calibrating a computational model of the whole system, including the motor, the pump and the hydraulic setting.

## 2. DATA AND METHODS

### 2.1. Experimental test bench

The main characteristics as well as the layout of the experimental test bench are detailed in (Hardy et al, 2021). All quantities measured with the main sensors are noted in Table 1 with their corresponding accuracy.

**Table 1.** Main measured quantities in the test bench

NOTATION	UNITS	Physical meaning	Accuracy
$\tilde{Q}^*$	m <sup>3</sup> /s	Measured flow rate	0.4%
$\tilde{H}_p^*$	m	Measured pump head	0.075%
$\tilde{P}_e^*$	W	Measured electrical power	0.5
$\tilde{\eta}_{tot}^*$	-	The total efficiency is estimated by the formula: $\tilde{\eta}_{tot}^* = \frac{\rho g \tilde{H}_p^* \tilde{Q}^*}{\tilde{P}_e^*}$	0.975%

A test procedure is established to draw characteristic curves of the pump with associated performance for nominal and off-design operation. To this aim, both the head losses and the rotation speed is tuned. The procedure is as follow:

1. **Install pump:** Submersible pumps to be tested are placed inside the tank through the door using a fork truck lift machine and the bridge crane installed at the top of the tank while dry-action pumps are placed inside laboratory;

2. **Fill the tank:** the tank is filled using laboratory pump through DN100 pipes;
3. **Bleed air in the pipes:** the pump test bench is bled everywhere in the bench where air is entrapped, i.e in P11, P21 and P3. A vacuum device using Venturi principle is used to vacuum the pipe P3 since this one is above the free surface inside the tank;
4. **Start a test:** to draw characteristic curves of the tested pump, two variables need to be systematically varied: the head losses and the rotation speed (via the frequency applied on the pump motor). A valve is used to generate the desired head losses and a variable frequency drive is used to control the rotation speed. The pump is started smoothly at a quite low rotation speed, with the lowest opening angle of the valve. It corresponds to state [0] in Figure 1. While the variables in the bench are continuously measured at a high frequency, the opening angle is increased by a step of  $\Delta A$ , up to the maximum flow rate of the pump or the valve maximum opening angle is reached, state [1] in Figure 1. Then, the operation is repeated in reversed order, by decreasing the valve opening angle to check previous measurements, state [2] in Figure 1. Next, the pump rotating speed is increased by increasing the frequency by a predefined step  $\Delta f$ , state [3] in Figure 1 and the whole operation is repeated again until the maximum frequency is applied. Then, the pump is stopped, state [4] in Figure 1. The valve is fully open and the pump can be changed.

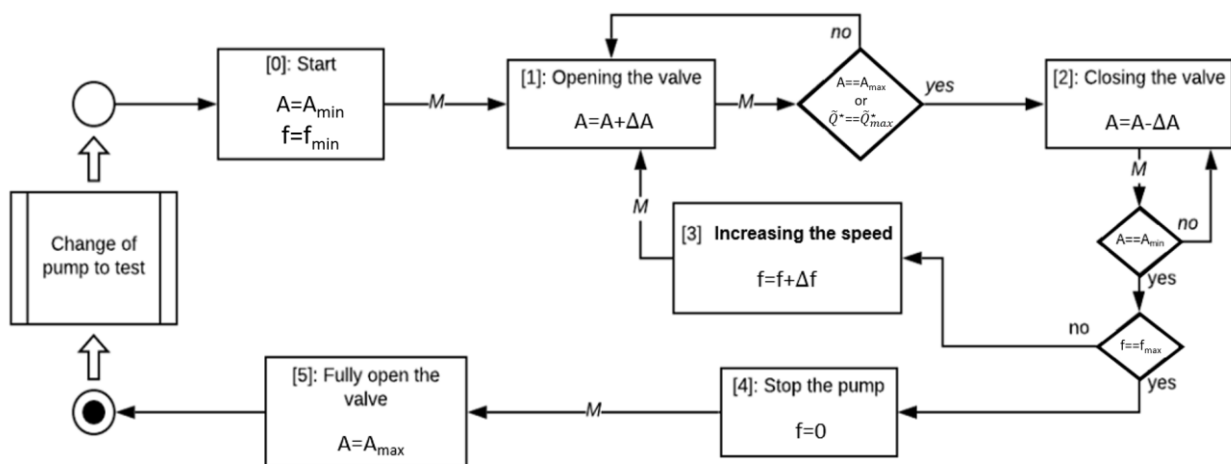


**Figure 1.** Block diagram of the testing procedure with five states using the following notations: A (the opening angle of the regulating valve; and  $\Delta A$ , the increment of opening angle); f (the frequency; and  $\Delta f$ , the increment of frequency);  $\tilde{Q}^*$  (the measured flow rate); and M (a Boolean value continuously checked, which is set to true if the measurements are steady during a time  $\Delta t$ ).

## 2.2. Governing equations

The model simulates, in steady-state, the motor operation (assuming an induction motor), the pump wheel operation and the head losses in suction and discharge pipes. The model inputs are the frequency  $\omega_s$ , the voltage  $e_x$  applied to the windings of the motor (as a function of the connection type: either star [220 V] or delta [400 V] with a three-phase voltage of 400 V between phases) and the hydraulic configuration i.e, the head difference  $H_e$  and the head loss coefficient  $c_f$ . The model computes the operation point of the pump: currents  $I$ , magnetic fluxes  $\psi$ , voltage  $V$ , ... and particularly the flow rate  $Q$ , the head  $H$  and the efficiencies of pump  $\eta_p$ , motor  $\eta_m$ , hydraulic efficiency  $\eta_h$  and overall efficiency  $\eta_{tot}$ .

To make the model formulation dimensionless, a number of characteristic quantities (also called base values) are defined, as detailed in Table 2. All variables are divided by their corresponding base value (subscript  $\square_B$ ) to formulate dimensionless equations.

**Table 2.** Base values used for the asynchronous motor driving the pump. Notification  $f_B$  stands for the nominal frequency,  $P_n$  the nominal electric power,  $PF$  the power factor,  $V_B$  the nominal voltage,  $H_p(Q = 0)$  the pump head for a zero flow rate and  $p$  the number of pairs of poles.

Units	Basis
Time [s]	$t_B = \frac{1}{\omega_B} = \frac{1}{2\pi f_B}$
Power [VA]	$S_B = \frac{P_n}{PF}$
Voltage [V]	$V_B$
Current [A]	$I_B = \frac{S_B}{3V_B}$
Impedance [ $\Omega$ ]	$Z_B = \frac{3V_B^2}{S_B}$
Flux [Wb]	$\psi_B = V_B t_B$
Rotor speed [ $s^{-1}$ ]	$\omega_{mB} = \frac{\omega_B}{p}$
Torque [Nm]	$T_B = \frac{S_B}{\omega_{mB}}$
Head [m]	$H_B = H_p(Q = 0)$
Flow rate [ $m^3/s$ ]	$Q_B = \frac{S_B}{\rho g H_B}$

The dimensionless equations constituting the model are:

$$0 = R_s i_{ds} + \omega_s \psi_{qs}; \quad (1)$$

$$e_x = R_s i_{qs} - \omega_s \psi_{ds}; \quad (2)$$

$$0 = R_r i_{dr} + (\omega_s - \omega_r) \psi_{qr}; \quad (3)$$

$$0 = R_r i_{qr} - (\omega_s - \omega_r) \psi_{dr}; \quad (4)$$

$$\psi_{ds} = L_{ss} i_{ds} + L_{sr} i_{dr}; \quad (5)$$

$$\psi_{qs} = L_{ss} i_{qs} + L_{sr} i_{qr}; \quad (6)$$

$$\psi_{dr} = L_{sr} i_{ds} + L_{rr} i_{dr}; \quad (7)$$

$$\psi_{qr} = L_{sr} i_{qs} + L_{rr} i_{qr}; \quad (8)$$

$$0 = (\psi_{dr} i_{qr} - \psi_{qr} i_{dr}) - (A_{fr} \omega_r + B_{fr} \omega_r^2) - (dQ^2 + eQ\omega_r + f_* \omega_r^2); \quad (9)$$

$$H_p = aQ^2 + bQ\omega_r + c\omega_r^2; \quad (10)$$

$$H_p = H_e + c_f Q^2; \quad (11)$$

where the subscripts  $d$ ,  $q$ ,  $s$  and  $r$  relate to the  $d$  axis of the Park transformation (Fitzgerald et al., 2003), the  $q$  axis of the Park transformation, the stator and the rotor. The 8 first equations model the behavior of an induction motor as described by Leonhard (2001). The parameters of the model are listed in Table 3. Their values are specific to each pump and should be identified experimentally. The standard ranges of variations of their dimensionless form are given in Table 4 (Van Cutsem, 2019). The input data of the numerical model are detailed in Table 5. The resolution of the 11 equations allows computing the 11 unknowns listed in Table 6.

**Table 3.** Parameters of the pump numerical model

Dimensional quantities		Dimensionless quantities	Physical meaning
NOTATION	UNITS		
$\tilde{R}_s$	$\Omega$	$R_s = \tilde{R}_s / Z_B \geq 0$	Stator winding resistance
$\tilde{R}_r$	$\Omega$	$R_r = \tilde{R}_r / Z_B \geq 0$	Rotor winding resistance
$\tilde{L}_{ss}$	H	$L_{ss} = \tilde{L}_{ss} / (Z_B t_B) \geq 0$	Equivalent inductance of the stator
$\tilde{L}_{sr}$	H	$L_{sr} = \tilde{L}_{sr} / (Z_B t_B) \geq 0$	Equivalent mutual inductance
$\tilde{L}_{rr}$	H	$L_{rr} = \tilde{L}_{rr} / (Z_B t_B) \geq 0$	Equivalent inductance of the rotor
$\tilde{A}_{fr}$	Nm s	$A_{fr} = \frac{\tilde{A}_{fr} \omega_{mB}}{T_B} \geq 0$	Coefficient modelling the viscous friction inside the motor

$\tilde{B}_{fr}$	Nm s <sup>2</sup>	$B_{fr} = \frac{\tilde{B}_{fr}\omega_{mB}^2}{T_B} \geq 0$	Coefficient modelling the friction inside the motor between rotor and air; and between the inner ring of the ball bearing and oil.
$\tilde{a}$	m <sup>-5</sup> s <sup>2</sup>	$a = \tilde{a}Q_B^2/H_B$	Coefficients used to compute the pump head as a parabolic function of the flow rate
$\tilde{b}$	m <sup>-2</sup> s <sup>2</sup>	$b = \tilde{b}Q_B\omega_{mB}/H_B$	
$\tilde{c}$	m s <sup>2</sup>	$c = \tilde{c}\omega_{mB}^2/H_B \geq 0$	
$\tilde{d}$	Nm <sup>-5</sup> s <sup>2</sup>	$d = \tilde{d}Q_B^2/T_B$	Coefficients used to compute the pump torque as a parabolic function of the rotation speed
$\tilde{e}$	Nm <sup>-2</sup> s <sup>2</sup>	$e = \tilde{e}Q_B\omega_{mB}/T_B$	
$\tilde{f}_*$	Nm s <sup>2</sup>	$f_* = \tilde{f}_*\omega_{mB}^2/T_B \geq 0$	

**Table 4.** Range of dimensionless parameter on the machine base

$R_s$	0.01 – 0.12	$R_r$	0.01 – 0.13
$L_{ss} - L_{sr}$	0.07 – 0.15	$L_{rr} - L_{sr}$	0.06 – 0.18
$L_{sr}$	1.8 – 3.8		

**Table 5.** Input data of the pump numerical model

Dimensional quantities		Dimensionless quantities	Physical meaning
NOTATION	UNITS		
$\tilde{\omega}_s$	Hz	$\omega_s = \tilde{\omega}_s/f_B \geq 0$	Frequency applied to the motor
$\tilde{e}_x$	V	$0 \leq e_x = \tilde{e}_x/(V_B) \leq 1$	Voltage applied to the motor
$\tilde{c}_f$	m <sup>-5</sup> s <sup>2</sup>	$c_f = \frac{\tilde{c}_f Q_B^2}{H_B} \geq 0$	It is a coefficient to compute the total head losses and is given by the sum of all head losses coefficient $k$ in suction and discharge pipes: $\tilde{c}_f = \sum_i \frac{k_i}{gA_i^2}$ with $k_i$ , the head losses coefficient of the $i^{\text{th}}$ part of the pipes; $g$ (9.81 m/s <sup>2</sup> ) and $A_i$ , the section of the $i^{\text{th}}$ part of the pipes.
$\tilde{H}_e$	m	$H_e = \tilde{H}_e/H_B \geq 0$	The head difference between navigation reach

**Table 6.** Unknowns of the pump numerical model

Dimensional quantities		Dimensionless quantities	Physical meaning
NOTATION	UNITS		
$\tilde{i}_{ds}$	A	$i_{ds} = \frac{\tilde{i}_{ds}}{\sqrt{3}I_B}$	Current in the stator fictive Park winding 'd'
$\tilde{i}_{qs}$	A	$i_{qs} = \frac{\tilde{i}_{qs}}{\sqrt{3}I_B}$	Current in the stator fictive Park winding 'q'
$\tilde{i}_{dr}$	A	$i_{dr} = \frac{\tilde{i}_{dr}}{\sqrt{3}I_B}$	Current in the rotor fictive Park winding 'd'
$\tilde{i}_{qr}$	A	$i_{qr} = \frac{\tilde{i}_{qr}}{\sqrt{3}I_B}$	Current in the rotor fictive Park winding 'q'
$\tilde{\psi}_{ds}$	Wb	$\psi_{ds} = \frac{\tilde{\psi}_{ds}}{\sqrt{3}\psi_B}$	Magnetic flux entering in the stator fictive Park winding 'd'
$\tilde{\psi}_{qs}$	Wb	$\psi_{qs} = \frac{\tilde{\psi}_{qs}}{\sqrt{3}\psi_B}$	Magnetic flux entering in the stator fictive Park winding 'q'
$\tilde{\psi}_{dr}$	Wb	$\psi_{dr} = \frac{\tilde{\psi}_{dr}}{\sqrt{3}\psi_B}$	Magnetic flux entering in the rotor fictive Park winding 'd'

$\tilde{\psi}_{qr}$	Wb	$\psi_{qr} = \frac{\tilde{\psi}_{qr}}{\sqrt{3}\psi_B}$	Magnetic flux entering in the rotor fictive Park winding 'q'
$\tilde{\omega}_r$	rad/s	$\omega_r = \tilde{\omega}_r/\omega_{mB}$	Rotational speed of the rotor (same as pump)
$\tilde{Q}$	m <sup>3</sup> /s	$Q = \tilde{Q}/Q_B \geq 0$	Flow rate supplied by the pump
$\tilde{H}_p$	m	$H_p = \tilde{H}_p/H_B \geq 0$	Pump head

Equation (9) expresses a torque balance where the electric torque  $T_e$ , a motor friction torque  $T_{fr}$  and the pump torque  $T_p$  are given by:

$$T_e = \psi_{dr}i_{qr} - \psi_{qr}i_{dr}; \quad (12)$$

$$T_{fr} = A_{fr}\omega_r + B_{fr}\omega_r^2; \quad (13)$$

$$T_p = dQ^2 + eQ\omega_r + f_*\omega_r^2. \quad (14)$$

This second torque models a viscous friction (Guedelha et al., 2019) as can appear in ball bearing fitted with friction seals, and the drag in air and in bearing lubrication proportional to the square of the velocity (Lathrop D.P., 1992). For simplicity, static friction is not considered. The pump head curve is assumed to follow a quadratic expression of the flow rate (Janevska, 2013) and the pump torque is expressed here as a second degree polynomial of the rotation speed (Van Cutsem et al., 1998; Engineering ToolBox, 2008). The derivation of the pump torque and head equations may be obtained using the affinity law (Stewart, 2019) and a torque expression introduced by MathWorks (2021).

Several efficiencies can be evaluated once the numerical model is solved:

$$\eta_m = \frac{T_p\omega_r}{e_x i_{qs}}; \quad (15)$$

$$\eta_p = \frac{H_p Q}{T_p\omega_r}; \quad (16)$$

$$\eta_h = \frac{H_e}{H_p}; \quad (17)$$

$$\eta_{tot} = \eta_m \eta_p \eta_h; \quad (18)$$

The motor efficiency  $\eta_m$  (15) is the ratio between its power consumption and the mechanical power given to the pump wheel. The pump efficiency  $\eta_p$  (16) is defined as the hydraulic power generated over the mechanical power provided by the motor. The hydraulic efficiency  $\eta_h$  (17) is the ratio between the targeted head difference  $H_e$  and the total head difference which includes head losses and is equal to the pump head  $H_p$ . The overall efficiency  $\eta_{tot}$  (18) is the product of these three parts.

The control strategy based on the variable speed drive is considered here to lead to  $e_x/\omega_s = 1$ .

### 2.3. Calibration procedure

The calibration of the numerical model is performed based on a non-linear optimization technic, namely the interior point method using the gradient as the direction and a Nelder-Mead optimization method to find the appropriate step. The goal of the calibration is to find the parameters of the model leading to numerical outcomes as close as possible to the real operating conditions measured during a pump test. Based on the conducted measurements, it is impossible to identify separately the coefficients  $B_{fr}$  and  $f_*$ . As shown in (9), only their sum can be identified. For the sake of simplicity, we set here  $B_{fr}$  to 0 and we consider only parameter  $f_*$ .

The method requires an initial guess of parameters given in Table 7. The subscript  $\square_{app}$  denotes an approximation of the coefficients  $a$  to  $f_*$ . The six first parameters are arbitrarily chosen within their standard range of variation, as given in Table 4. A relatively low value was taken for coefficient  $A_{fr}$  which represents motor internal friction. Since all quantities are dimensionless in the numerical model, the measurements recorded in a pump test are divided by their corresponding basis ( $Q_B$  and  $S_B$ ) and denoted by the upper script  $\square^*$ .

**Table 7.** Initial guess of the numerical model parameters for the calibration procedure

$R_s$	$R_r$	$L_{ss}$	$L_{sr}$	$L_{rr}$	$A_{fr}$
0.02	0.02	2.2	2.1	2.2	1e-4
$a$	$b$	$c$	$d$	$e$	$f_*$
$a_{app}$	$b_{app}$	$c_{app}$	$d_{app}$	$e_{app}$	$f_{app}$

The initial guesses  $a_{app}, b_{app}, c_{app}, d_{app}, e_{app}$  and  $f_{app}$  are obtained based on these two assumptions:

$$\omega_r = 0.9 \omega_s^* \quad (19)$$

$$T_p = \frac{P_e^*}{\omega_s^*} \quad (20)$$

These equations are valid for operation conditions close to the nominal ones. Thereby, the rotation speed is almost equal to the synchronous speed and the motor efficiency is considered equal to 90%, which leads to (20). The efficiency of variable speed drive is assumed equal to 100%. Introducing these assumptions into (10) and (14) enables ending up with a set of linear expressions, which can be solved for the coefficients using a linear least square method:

$$H^* = a_{app}(Q^*)^2 + b_{app}Q^*0.9\omega_s^* + c_{app}(0.9\omega_s^*)^2 \quad (21)$$

$$\frac{P_e^*}{\omega_s^*} = d_{app}(Q^*)^2 + e_{app}Q^*0.9\omega_s^* + f_{app}(0.9\omega_s^*)^2 \quad (22)$$

Next, a non-linear optimization problem is solved to calibrate the numerical model based on  $N_p$  measured operating points. The objective function is:

$$\min \Theta(\bar{x}_p) = \sum_{l=1}^{N_p} c_Q(Q_l - Q_l^*)^2 + (1 - c_Q)(e_{x,l}i_{qs,l} - P_{e,l}^*)^2 \quad (23)$$

where the subscript  $l$  refers to the measurements and the equivalent outcomes of the numerical model for a same input configuration  $(\omega_{s,l}^*, H_l^*)$ , from 1 to  $N_p$ . The inputs for each measurement are given as  $(\omega_s = \omega_{s,l}^*; e_x = \omega_{s,l}^*; H_e = H_l^*; c_f = 0)$ . The objective function (23) aims at minimizing a weighted sum of the squared flow rate deviation of the numerical model from the experimental measurements and the squared power consumption deviation. Coefficient  $c_Q$  varies in the interval  $[0, 1]$  and is a parameter of the optimization. It plays the role of a weight to prioritize the accuracy of the flow rate compared to the power consumption or vice-versa. The numerical model called  $N_p$  times could have been considered as equality constraints. Nevertheless, as this amount of equality constraints (11 equations for all  $N_p$  measurements leading to  $11N_p$  equations) are huge, they are not considered in the optimization process to build the Lagrangian function. Instead, the only variables of the optimization are the model parameters  $\bar{x}_p = (R_s, R_r, L_{ss}, L_{sr}, L_{rr}, A_{fr}, a, b, c, d, e, f_*)$ . For each optimization iteration, the numerical model is called with model parameters corresponding to the iterate of the optimization process for all  $N_p$  configurations.

The inequality constraints are:

$$\bar{c}(\bar{x}_p) \geq \bar{0} \quad \left\{ \begin{array}{l} 0.01 < R_s < 0.12 \quad (24) \\ 0.01 < R_r < 0.12 \quad (25) \\ 0.07 < L_{ss} - L_{sr} < 0.15 \quad (26) \\ 1.8 < L_{sr} < 3.8 \quad (27) \\ 0.06 < L_{rr} - L_{sr} < 0.15 \quad (28) \\ 0 < A_{fr} < 0.2 \quad (29) \\ a \in [0; 2a_{app}] \text{ or } [2a_{app}; 0] \quad (30) \\ b \in [0; 2b_{app}] \text{ or } [2b_{app}; 0] \quad (31) \\ c \in [0; 2c_{app}] \text{ or } [2c_{app}; 0] \quad (32) \\ d \in [0; 2d_{app}] \text{ or } [2d_{app}; 0] \quad (33) \\ e \in [0; 2e_{app}] \text{ or } [2e_{app}; 0] \quad (34) \\ f_* \in [0; 2f_{app}] \text{ or } [2f_{app}; 0] \quad (35) \end{array} \right.$$

and can be gathered under the notation  $\bar{c}$ . The five first inequalities come from literature (Van Cutsem T., 2019). Equation (29) is a relatively large interval that hardly influences the optimization as the actual value of  $A_{fr}$  is expected to remain low (since it expresses the rotational friction inside the motor). The bounds of the last six coefficients are fixed arbitrarily to twice the approximated coefficients obtained by applying the least square identification method according to (21) and (22). This last choice offers a quite large range of variation for these six coefficients and should be enough since the approximations obtained  $\square_{app}$  are probably not far from the real coefficients that the calibration should return.

In terms of resolution, four additional coefficients are introduced to guide the calibration. Hence, five coefficients may influence the way the optimization under constraints behaves. These are described in Table 8. The optimization technic performed is described in Figure 2. Ultimately, at the end, an optimization is performed without constraints with as guess, the final  $\bar{x}_p$  obtained in the calibration under constraints.

**Table 8.** Parameters of optimization to calibrate the pump model

Notation	Default value	Meaning
$c_Q$	0.5	Homotopy coefficient that varies in the interval [0, 1] and is a parameter of the objective function. It plays the role of a weight to prioritize the accuracy of the flow rate compared to the power consumption when greater than 0.5.
$Tol$	1e-4	It gives the tolerance at which the optimization could stop. The criterion is: $\ \bar{x}_{p,i} - \bar{x}_{p,i-1}\  < Tol$
$t_{IP}$	100	This parameter is the first gain applied to the constrains. The smaller the more the constrains influence the direction of the path to the best parameters $\bar{x}_p$ .
$dX$	1e-7	The variation of parameter used to estimate the derivative of the objective function with respect to the parameters. Fortunately, since the numerical model is dimensionless, a same variation could be used for each parameters.
$Tol_{NM}$	1e-7	The tolerance that the Nelder-Mead method should have to estimate the optimal step to approach a minimum.

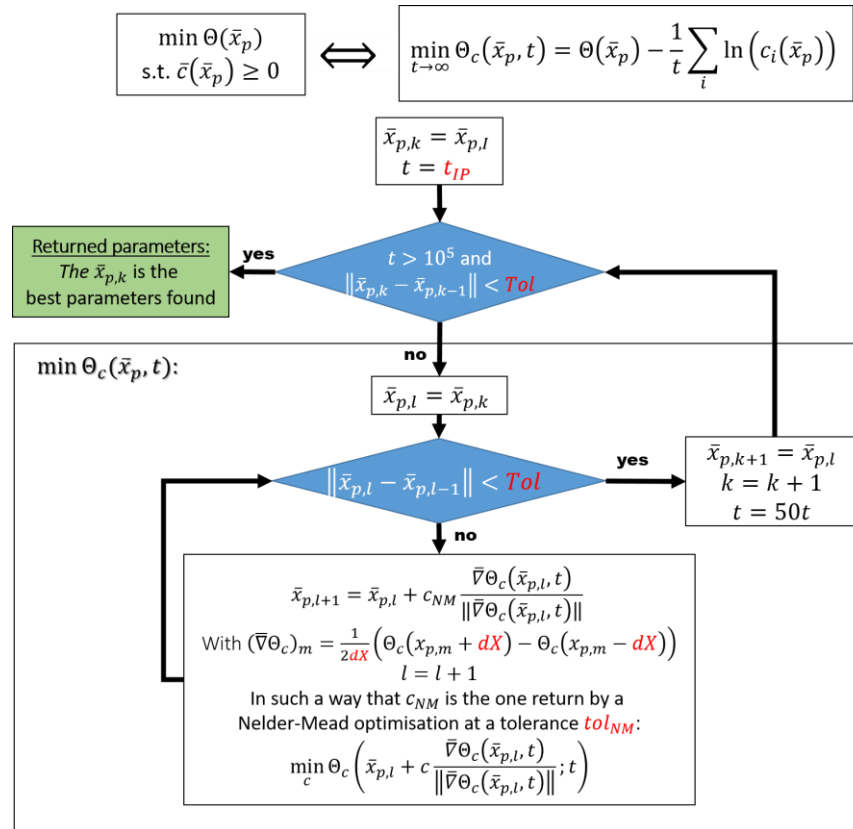


**Figure 2.** Numerical resolution of the calibration problem emphasizing the role of each computational parameters of Table 8

### 3. RESULTS

#### 3.1. Experimental observation

The pump used to demonstrate our procedure is an Amarex centrifugal submersible pump. Its main operating characteristics are listed in Table 9. The manufacturer provides a pump curve for the nominal frequency and voltage. Based on these information, the machine base introduced in section 2.2, can be obtained in Table 10 for the Amarex pump.

**Table 9.** Operating characteristics of the 'Amarex KRT D 250 - 400/206UG-S' pump

Flow rate	170 l/s	Nominal voltage ( $V_B$ )	400 V
Head	6.00 m	Nominal frequency ( $f_B$ )	50 Hz
Operating speed	965 RPM	Nominal electrical power ( $P_n$ )	18 kW
Absorbed power	14.03 kW	Nominal current	35.5 A
Efficiency	71.7 %	Nominal efficiency	87 %
Number of pair of poles ( $p$ )	3	Nominal power factor ( $PF$ )	0.85

**Table 10.** Basis used for the Amarex pump to pass in per unit system.

Units	Basis
Time	$t_B = \frac{1}{\omega_B} = \frac{1}{2\pi f_B} = 3.18 \text{ ms}$
Power	$S_B = \frac{P_n}{PF} = \frac{18}{0.85} = 21.18 \text{ kVA}$
Voltage	$V_B = 400 \text{ V}$
Current	$I_B = \frac{S_B}{3V_B} = 17.65 \text{ A}$
Impedance	$Z_B = \frac{3V_B^2}{S_B} = 22.67 \Omega$
Flux	$\psi_B = V_B t_B = 1.27 \text{ Wb}$
Rotor speed	$\omega_{mB} = \frac{\omega_B}{p} = 1000 \text{ RPM}$
Torque	$T_B = \frac{S_B}{\omega_{mB}} = 202.22 \text{ Nm}$
Head	$H_B = H_p(Q = 0) = 14 \text{ m}$
Flow rate	$Q_B = \frac{S_B}{\rho g H_B} = 154.2 \text{ l/s}$

The 51 measuring points ( $N_p=51$ ) obtained during the test of the Amarex pump are drawn in Figure 3. The head-(flow rate) curve with a 50 Hz motor excitation, is 0.7 m (RMS value) below the datasheet displayed in dashed line. The difference could be due to the storage of the pump outside during several years. The manufacturer efficiency drawn in Figure 3b is not well defined. There is no information to know whether it includes the motor efficiency. Assuming that it does, the dashed curve may be interpreted as the total efficiency of the motor and pump together. The efficiencies provided by experimental data and by the datasheet differ by up to 10%.

### 3.2. Computational results

The experimental tests provide data on flow rates, heads and power consumptions for several motor excitations. The calibration procedure is then applied with the bench results to provide parameters to the numerical model. The parameters obtained are given in Table 11. The RMS<sup>1</sup> errors between computations and measurements are in average 6 %, 5 % and 7 % for the flow rate, the electric power and the total efficiency, with a SD<sup>2</sup> of 6 %, 5 %, 7 %.

The RMS relative error of the numerical model outcomes over the experimental data, are depicted by dots in Figure 4a classified by the frequency applied to the pump. In Figure 4b, the best efficiency point of the pump can be identified, quantitatively 145 l/s and 7m. The convergence of the objective function is displayed in Figure 5a where jumps of convergence are observed when  $t$  values are increased. The optimization parameters are studied in Figure 5b by varying each parameter and evaluating its impact on the RMS relative errors (color) and their SD (width). This confirms the validity of the optimization parameters retained in Table 8.

**Table 11.** Numerical model parameters identified in the calibration procedure with  $c_Q=0.5$

$a_{app}$	$b_{app}$	$c_{app}$	$d_{app}$	$e_{app}$	$f_{app}$
-0.1324	-0.3579	1.1039	-0.3481	0.6389	0.6660
$R_s$	$R_r$	$L_{ss}$	$L_{sr}$	$L_{rr}$	$A_{fr}$
0.12523	0.05905	2.14154	2.05823	2.14518	0.14887
$a$	$b$	$c$	$d$	$e$	$f$
-0.15581	-0.29619	0.96051	-0.17884	0.30918	0.39379

<sup>1</sup> RMS: Root Men Square

<sup>2</sup> SD: Standard Deviation

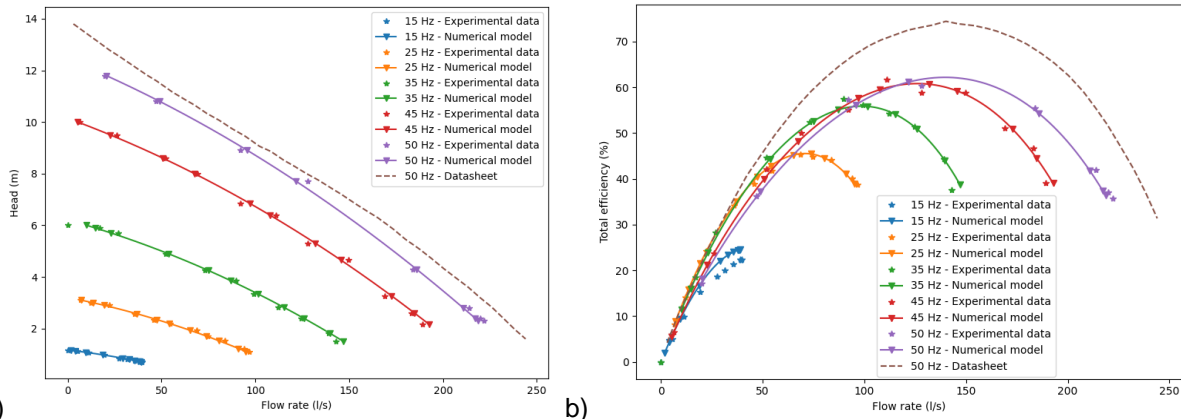


**Figure 3.** Comparison between pump curves provided by the bench measurements (star) and the numerical model (triangle)

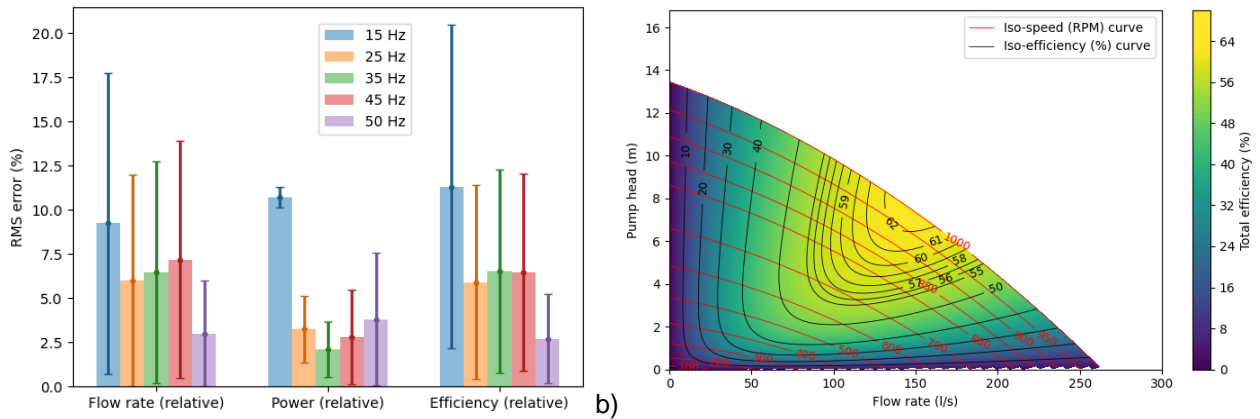


**Figure 4.** a) Distribution of the RMS relative error and standard deviation for flow rate, power consumption and total efficiency between numerical model and experimental results; b) Mapping of the overall efficiency of the pump for varied flow-rates, heads and rotation speed.

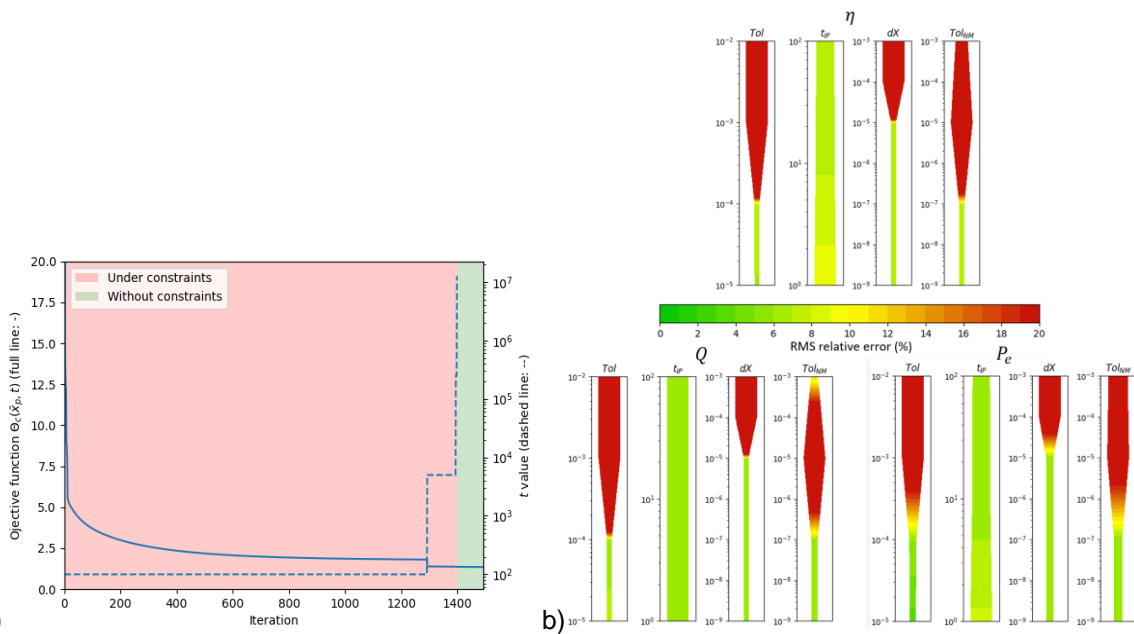


**Figure 5.** a) Objective function (full line) and value of  $t$  (dashed line) during the calibration; b) RMS error of the numerical model for the 51 measurements as a function of the four numerical optimization parameter introduced in Table 11 (the width is proportional to SD)

The calibration is performed for several coefficient  $c_Q$ . As seen in Figure 6, the errors obtained for the models with a calibration using  $c_Q \in [0.2; 0.7]$  are relatively similar. The main coefficients affected are  $d, e, A_{fr}$  and in a lesser degree,  $L_{rr} - L_{sr}, L_{ss} - L_{sr}, R_r$ .

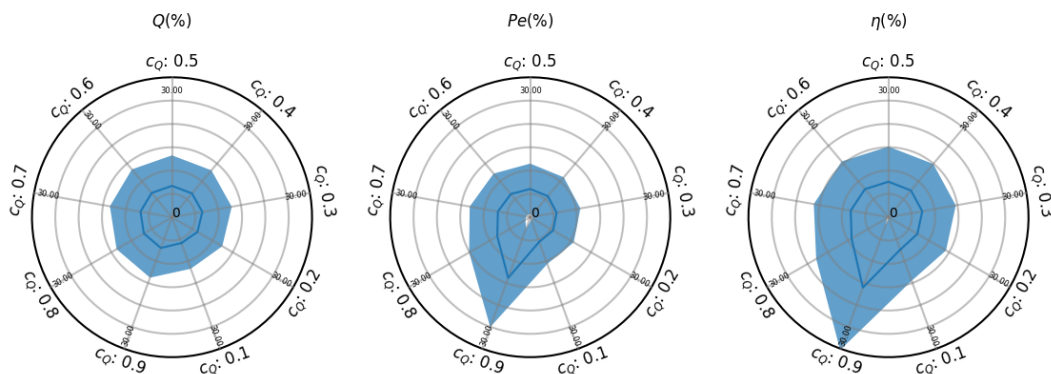


**Figure 6.** Influence of the coefficient  $c_Q$  in the objective function during the calibration (full line: RMS value; colored area: [RMS-SD; RMS+SD])

#### 4. CONCLUSIONS

Fairly accurate predictions of pump performance have been obtained for a broad range of operation conditions. The value of this combined experimental and numerical characterization of the pumps is to provide to the pump operator a full characterization of the pump performance, well beyond the nominal conditions which are usually reported by the manufacturer. It helps the pump operator assessing the loss of pump efficiency when it is operated in real-world conditions differing from the nominal ones. Repeating periodically this characterization enables assessing the effect of pump aging on its performance. A software is currently under development allowing pump users to obtain the operating values of their pump for different configurations by simulation. In a subsequent step of the research, the computational model will be coupled with a model of navigation channels.

#### 5. ACKNOWLEDGEMENTS

This research is partly supported by ERDF funding in the framework of the Interreg NWE project Green Win. Canal & River Trust is gratefully acknowledged for sharing data on the operation of the Kennet and Avon canal

#### 6. REFERENCES

- Engineering ToolBox. Centrifugal Pumps - Speed Torque Curve, 2008, [https://www.engineeringtoolbox.com/pumps-speed-torque-d\\_1114.html](https://www.engineeringtoolbox.com/pumps-speed-torque-d_1114.html);
- Fitzgerald E., Charles Kingsley. Jr., Stephen D. Umans. Electric Machinery, sixth edition. Book, pp. 664-667, 2003
- Guedelha N., Silvio T., and Daniele P. Identification of Motor Parameters on Coupled Joints. ArXiv: 1906.05070 [Cs], 2019, <https://arxiv.org/pdf/1906.05070.pdf>
- Hardy J., et al. Experimental Test Bench for Performance-Assessment of Large Submersible and Dry-Action Pumps Used in Waterways. Publ. Inst. Geophys. Pol. Acad. Sci. Geophys. Data Bases Process. Instrum. 434, pp. 101–103, 2021.
- Janevska G. Mathematical Modeling of Pump System. EIIIC the 2<sup>nd</sup> Electronic International Interdisciplinary Conference, Zilina, Czech Republic, 2013, [https://www.researchgate.net/publication/283348821\\_Mathematical\\_Modeling\\_of\\_Pump\\_System](https://www.researchgate.net/publication/283348821_Mathematical_Modeling_of_Pump_System)
- Lathrop D.P., Fineberg J. and Swinney H.L. Turbulent flow between concentric rotating cylinders at large Reynolds number. Physical Review Letters, Vol. 68, No. 10, pp. 1515-1518, 1992, <https://journals.aps.org/prl/pdf/10.1103/PhysRevLett.68.1515>
- Leonhard W. Control of Electrical Drives, third edition. Book, pp. 163-211, 2001
- MathWorks. Centrifugal pump. Documentation: Simscape, Fluids, Hydraulics (isothermal), Pumps and Motors; Description: Parameterizing the Pump by Approximating Polynomial; R2021b, <https://www.mathworks.com/help/phymod/hydro/ref/centrifugalpump.html>.
- Stewart M. 3 - Centrifugal pumps. Surface Production Operations, Gulf Professional Publishing, section 3.6.2, pp. 120-124, ISBN 9780128098950, 2019, <https://doi.org/10.1016/B978-0-12-809895-0.00003-X>.
- Van Cutsem T., Vournas C. Voltage Stability of Electric Power System. New York, Springer, pp. 100-113, 1998
- Van Cutsem T. Power systems dynamics, control and stability, Dynamics of the induction machine, course, sl.9, 2019, <https://thierryvancutsem.github.io/home/courses.html>